

# SUTD-PRCM Dataset and Neural Architecture Search Approach for Complex Metasurface Design

Tianning Zhang<sup>1</sup>, Yee Sin Ang<sup>1</sup>, Erping Li<sup>2</sup>, Chun Yun Kee<sup>1,\*</sup>,  
L. K. Ang<sup>1,\*</sup>

<sup>1</sup>Science, Mathematics and Technology, Singapore University of Technology and Design (SUTD), 8 Somapah Road, Singapore 487372

<sup>2</sup> College of Information Science and Electronic Engineering, Zhejiang University, Hangzhou 310027, China

\*Authors to whom any correspondence should be addressed

E-mail: chunyun\_kee@sutd.edu.sg, ricky\_ang@sutd.edu.sg

**Abstract.** Metasurfaces have received a lot of attentions recently due to their versatile capability in manipulating electromagnetic wave. Advanced designs to satisfy multiple objectives with non-linear constraints have motivated researchers in using machine learning (ML) techniques like deep learning (DL) for accelerated design (forward and inverse) of metasurfaces. For metasurfaces, it is difficult to make quantitative comparisons between different ML models without having a common and yet complex dataset used in many disciplines like image classification. Many studies were directed to a relatively constrained datasets that are limited to specified patterns or shapes in metasurfaces. In this paper, we present our SUTD polarized reflection of complex metasurfaces (SUTD-PRCM) dataset, which contains approximately 260,000 samples of complex metasurfaces created from electromagnetic simulation, and it has been used to benchmark our DL models. The metasurface patterns are divided into different classes to facilitate different degree of complexity, which involves identifying and exploiting the relationship between the patterns and the electromagnetic responses that can be compared in using different DL models. With the release of this SUTD-PRCM dataset, we hope that it will be useful for benchmarking existing or future DL models developed in the ML community. We also propose a classification problem that is less encountered and apply neural architecture search (NAS) to have a preliminary understanding of potential modification to the neural architecture that will improve the prediction by DL models. Our finding shows that convolution stacking is not the dominant element of the neural architecture anymore, which implies that low-level features are preferred over the traditional deep hierarchical high-level features thus explains why deep convolutional neural network based models are not performing well in our dataset (SUTD-PRCM dataset).

## 1. Introduction

Due to the interaction between an electromagnetic (EM) wave and metasurfaces in some specific geometrical arrangements, metasurfaces can exhibit remarkable electromagnetic wave responses that have attracted great interests [1–4]. Metasurfaces have served as an important technology in many applications such as heat transforming [5], cloaking [6, 7], hologram [8], conversion [9], absorption [10, 11], scattering reduction [12], polarization [13–15], transmission [16], color [17, 18], metalense [14, 15], programmable metasurfaces [19–21], and many others [22–25]. These applications are made possible by the rapid advancement in micro- and even nano- fabrication technologies and computational modeling over the past decades. In the design of complex metasurfaces, machine learning (ML) methods like deep learning (DL) techniques has demonstrated unprecedented performance in providing rapid yet accurate prediction [26]. Particularly, DL technique has been mainly applied for forward modeling and inverse design generation [27–30]. For forward modeling, instead of solving explicitly the governing Maxwell equations, DL models are capable of learning the complex non-linear mapping between input parameters to output EM response for a sufficiently large and high-quality dataset. The resulting high fidelity surrogate model can readily replace the costly numerical solvers in the traditional design methodology based on evolutionary algorithms such as genetic algorithm (GA) [31], particle swarm optimization (PSO) [32], and ant colonization optimization (ACO) [33]. Compared to computationally expensive numerical solvers, efficient and accurate evaluation of DL surrogate model can lead to faster computational time and larger design search dimensions. In the inverse design, the generative model of desirable metasurfaces can be based on DL model with the desirable EM response as an input. For a generative adversarial network (GAN) system, training of the generative model will involve a forward model which can be either numerical solvers or DL models. Similarly, replacing the forward model by a accurate and efficient DL model can lead to tremendous speed up in terms of training. Nowadays, with metasurface designs typically represented as digital images, the most commonly adopted neural architectures in DL are deep convolutional neural network (DCNN) which is proven effective in various computer vision (CV) related problems.

All the advantages mentioned requires a good and if possible common dataset of metasurfaces to benchmark different DL models used in the community. The involvement of DL typically started from the exploration with the most basic neural architecture, a fully connected network (FCN) [34–36] for supervised learning. With this approach, the electromagnetic scattering behaviour of an alternating dielectric thin films parameterized on thicknesses and dielectric constants of the films were successfully predicted [37]. In dealing with the instability and inconsistency problem, a bidirectional encoder-decoder model (Tandem) is proposed [37]. The perception of treating metasurfaces as images has led to seamless introduction of convolutional neural network (CNN) into metasurface design allowing 2D image as input. A recent paper [38] studied this problem when the output is only a scalar parameter. ML algorithm

on densely sampled spectral output such as reflection and transmission were also tested [39, 40]. For inverse design, deep generative models are employed for generating new meta-atom designs to achieve the desired EM response. Various groups [39, 41] have used GAN system to quantify a differential mapping from desired EM response to the discrete 2D pattern. In a recent paper [42], contrast-vector is used to emphasize on the location of spectral peak in order to improve the performance of inverse design. Another paper [43] further enhances the expression capability of the DL model by appending to CNN a recurrent neural network (RNN) which is more often seen in sequence modeling.

However, we observe that majority of the DL related works in metasurface design are restricted to canonical shapes or connected polygon which belong to a relatively simple and limited design dimension. The findings reported in using such limited dataset are also qualitative at best in the comparison of different neural architectures. It is less intuitive to make meaningful comparison across different models without a common and more complex dataset. Easy access to such standard dataset will allow a more quantitative and fair comparison between different neural architectures and training strategies in the research community. Inspired by how the standard datasets in CV community has advanced the state-of-the-art in their field, we are ready to share our dataset (SUTD-PRCM), which was first generated in a previous work and tested on different DL models [44]. This dataset is essentially a collection of numerical simulated results of EM wave reflection of randomly created metasurfaces. Each sample in the dataset consists of an input metasurface of 16 x 16 binary image, and its associated output EM reflection as a function of frequency from 2 to 10 GHz. The randomly generated samples are sufficiently complex that are suitable for forward prediction and inverse design in testing different DL models in a simple GPU. In our recent work [44], we have demonstrated that in using this SUTD-PRCM dataset tested with some existing DCNN based neural architectures that might not be the most optimal neural architecture yet. Thus this dataset is published here to share with the community for further testing.

For the first part of this paper, we introduce this SUTD-PRCM dataset in more details. We then present an automated approach to improve the architecture of DL models for better performance. For demonstration purpose, an application to a classification problem based on this dataset is considered. Note that the approach is general and it is likewise applicable to a regression problem [44]. Thus the objective of this paper is two folds. Firstly, we would like to share this physics based dataset (obtained by EM solvers) of metasurfaces with the community to explore future improvement in neural architecture for forward modeling and inverse design of such complex metasurface. Relevant resources including the dataset and code for retrieving the data are shared on Github. Secondly, we will elaborate on the implementation of network architecture search (NAS) using a classification problem based on this dataset. The paper is organized as follows. The second section presents the details of the SUTD-PRCM dataset. The third section introduces several formulations of machine learning problems based on this dataset and relevant treatments needed. The fourth section

considers one of the formulated ML problem in third section and NAS is applied to achieve better performance. Finally, we conclude the paper with a summary and possible future works.

## 2. The SUTD-PRCM dataset

Our SUTD-PRCM dataset was created by automating the full wave EM simulation with the SUMULIA CST Studio Suite and MATLAB to provide accurate characterization of randomly created metasurfaces. In this section, we will introduce the dataset by providing the details of the EM simulation and the characteristics of this dataset.

### 2.1. Generation of data

An input metasurface pattern,  $\mathcal{I}$ , is associated with a set of densely sampled EM spectral responses under a given setting:  $\mathcal{E}$ , which is described by a set of physical parameters such as material type (dielectric or metal), frequency range (GHz to THz), feature size, and others. Different settings of  $\mathcal{E}$  will led to different EM responses governed by the Maxwell equations. Therefore, a DL model can be perceived as a surrogate model that mimic the input/output behaviour of the complex systems governed by the Maxwell equations. If a DL model is trained properly with a sufficiently large and appropriate dataset, it can be used to predict the EM response (of particular application) without solving the Maxwell equations. Thus the quality of the dataset is the most important factor for DL models to function properly.

For the traditional methods, with the information of  $\mathcal{E}$  and the input pattern  $\mathcal{I}$ , one can obtain the EM response accurately and robustly via a numerical solver like rigorous coupled-wave analysis (RCWA), finite-difference time-domain method (FDTD), or finite element method (FEM). Here, we have adopted the FEM solver in CST Studio Suite to create the samples. Each sample of SUTD-PRCM is made up of an input of metasurface pattern,  $\mathcal{I}$ , and outputs of associated  $x$ - and  $y$ - polarized reflection. Each metasurface is represented by a unique pattern encoded by a  $16 \times 16$  matrix that made up of 0 and 1. The binary setting of 1 or 0 corresponds respectively to the presence or absence of a square copper patch (0.5 mm x 0.5 mm x 0.018 mm) on top of a dielectric substrate with  $\epsilon_r = 2.65 \times (1 + 0.003i)$  and  $\mu_r = 1$ , and it is backed by a 0.18-mm-thick copper plate. The sample has a padding of 1 mm on the sides which forms the unit cell used in the simulation. Simulations were performed with unit cell boundary condition in  $x$  and  $y$  direction and open boundary condition in the  $z$  direction. An  $x$ -polarized plane wave is incident normally from the top of the metasurface as illustrated in Fig.1. In general, the EM spectral responses include reflection and transmission of different polarizations. For simplicity, the metasurface under consideration is of pure reflective type (note such limitation can easily be changed in the code). Thus the EM spectral responses only contain  $x$ -polarized ( $\mathcal{R}$ ) and  $y$ -polarized ( $\mathcal{T}$ ) reflection associated with a given sample. Each spectrum is computed for frequency from 2 to 12 GHz sampled for 1001 points.

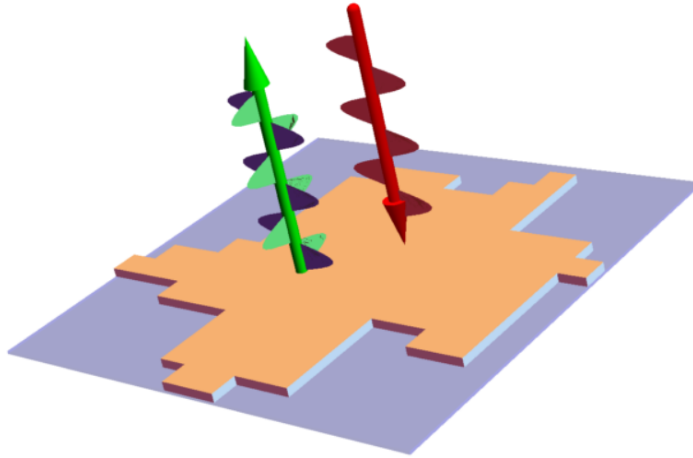


Figure 1: A  $x$ -polarized electromagnetic wave (red) incident on a purely reflective metasurface and the  $x$ - and  $y$ - polarized electromagnetic reflected wave (green).

We define  $\mathcal{C}_{f_i}^R$  and  $\mathcal{C}_{f_i}^T$  to be the numerical values (complex numbers) related to  $\mathcal{R}$  and  $\mathcal{T}$ , respectively, where  $f_i$  denotes the discrete frequency points. The fraction of reflected energy can be calculated from  $P = |\mathcal{C}_{f_i}^R|^2 + |\mathcal{C}_{f_i}^T|^2$ . Due to conservation of energy,  $P$  is capped at 1 and  $P < 1$  implies some energy absorption into the substrate.

## 2.2. Classes of metasurfaces

The patterns of metasurfaces are encoded into a binary matrix of size  $16 \times 16$ . Depending on the aggregation or configuration of the pixels (see Fig. 2 below), we divide the samples in the dataset into four classes: (a) Polygon-like (PLG), (b) Polygonal ring (PLR), (c) Pattern-combination (PTN), and (d) Random (RDN). The PLG class resembles filled polygon, which are connected topologically and can deform smoothly to each other. The PLG class is dense and are more commonly encountered in manufacturing type design [42, 43, 45]. The number of possible combinations of the PLG class is estimated to be about  $2^{152}$ . The PLR class resembles polygonal rings, which are formed by an enclosed area in between two cocentric polygons. Note the inner polygon of PLR class may vanish (zero pixel), for which PLR will become PLG. The PTN class contains patterns formed by combining disjointedly any number of the six basic shapes such as square (9 pixels), cross (5 pixels), triangle (4 pixels) of four directions, U-shape (5 pixels), and H-shape (7 pixels). The possible number of PTN class is estimated to be about  $2^{102}$ . Finally, the RDN class does not have any restriction, where the patterns are totally random binary images and thus has the highest number of combination at about  $2^{256}$ . Table 1 summarizes the characteristics of these 4 classes of metasurfaces with a total of 260,000 samples.

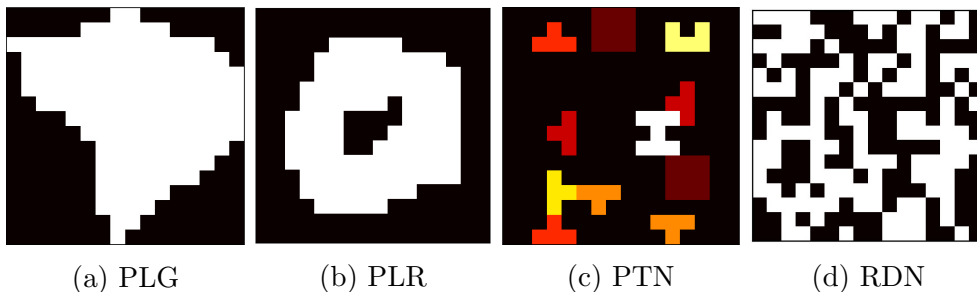


Figure 2: Samples of metasurface pattern from different classes.

Table 1: Classes of metasurface patterns.

Name	Samples	Description
<b>PLG</b>	<b>30000</b>	Polygon patterns
<b>PLR</b>	<b>60000</b>	Polygonal ring formed by two cocentric polygons
<b>PTN</b>	<b>60000</b>	Combination of squares, crosses, triangles, U-shapes, H-shapes
<b>RDN</b>	<b>110000</b>	Totally random binary patterns

### 2.3. Relationship between classes

Within the dataset, there is no overlapping samples between any two classes. However, the domain of the 4 classes are related. When the inner polygon in PLR class vanishes, the patterns resembles those in PLG, thus the domain of PLG class is a subset of the PLR class. Since the RDN class does not contain any restriction and cover all possible patterns allowed for a 16x16 binary image, the domain is a superset of the other 3 classes. Intuitively, we hope a DL model trained only by the RDN class of data is able to acquire sufficient information to allow equal prediction as compared to those trained separately by the other 3 classes (PLG, PLR, and PTN). If this goal is met, we will consider that the DL model is successful, which may be able to capture the underlying physics. Unfortunately, we have concluded in a recent study [44] that current CNN based DL models are insufficient to reach this optimal condition for which cross classes forward prediction shows deteriorating performance. We postulate that this is due to non-optimal neural architecture adopted, which motivates us to share our dataset in this paper with other researchers for future improvements.

## 3. Formulations of supervised learning task

In this section, we will demonstrate some formulations for supervised learning task based on the dataset. The goal is to establish a model, which is able to predict the reflection of both polarizations simultaneously. An obvious method is to consider the 2-branches of complex-valued output as a 4-branches of real-value output and use a gigantic model to model the data regardless of the model size, layers, and branches. However, it is always preferable to have a more compact and efficient model that leads to less memory

footprint and quicker calculation. To better study the ML algorithm’s behavior on this dataset, we present some simpler EM characteristics, which can be derived from the dataset.

### 3.1. Complex response

Instead of aiming to predict the reflection of both polarizations, divide and conquer can be a good strategy to get started. We focus on predicting just one polarization at a time, either the  $x$ - or  $y$ -polarized reflection. In doing so, the complex number based EM response still remains unconventional as compared to the traditional DL methods in dealing with real-number based datasets. Without a viable complex-valued neural network available to apply directly, an improvised solution is often to drop the phase information or to split the real and imaginary part into two separate components during the training process. Note that this is equivalent to ignoring the inherent relationship between the real and imaginary parts. This might not be the ideal approach (it is inconsistent in terms of physics) but we considered it is an adaptive measure to quickly tap into the existing DL models that we can use directly. We note that there is a growing interest in exploring the advantages of complex-valued neural networks [46], which may be used for our complex-number based SUTD-PRCM datasets shared here, and this will be studied in a future work.

### 3.2. Magnitude and phase spectrum

For simplicity, the complex-valued EM response from SUTD-PRCM dataset is converted into two real-number based representation of magnitude (Fig.3a) and phase (Fig.3b). In Fig. 3a, for a given RDN sample, we show the magnitude of  $x$ -polarized reflection ( $|\mathcal{R}|$ ),  $y$ -polarized reflection ( $|\mathcal{T}|$ ), and  $P = |\mathcal{T}|^2 + |\mathcal{R}|^2$  for a spectrum from 2 to 12 GHz. In Fig. 3b, we show the statistical plotting of the mean and variance of the phase for  $\mathcal{R}$  ( $x$ -polarization in blue) and  $\mathcal{T}$  ( $y$ -polarization in red). Within this dataset, the magnitude spectra are typically continuous and smooth. Compressed representations for these spectra are highly desirable in reducing the number of parameters, which will improve the efficiency of training and accuracy of model prediction. Fourier transform[23, 47], discrete cosine transform, wavelet transform and uniform down-sampling are some popular options in constructing compressed representations. In our prior work [44], we reported that uniform down-sampling has produced good results to predict the magnitude. However, the phase spectra are oscillatory due to the periodicity of  $2\pi$ . It is evident that the variance is high for the  $x$ -polarized reflection,  $\mathcal{R}$ . This behaviour can be problematic in training a DL model and leads to biased preference of real/imaginary representation in some studies.

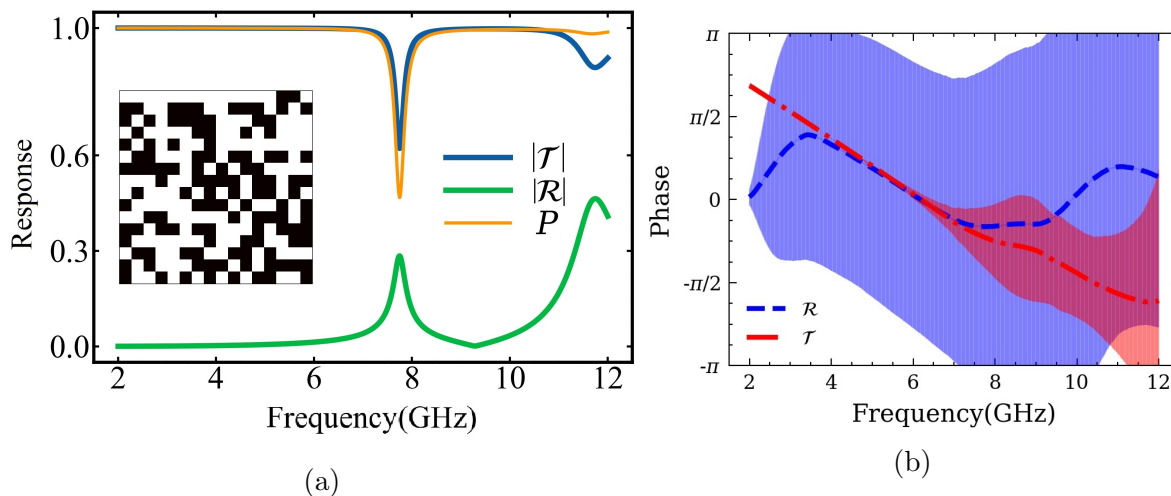


Figure 3: (a) Magnitude spectra of a RDN metasurface sample:  $|\mathcal{T}|$ ,  $|\mathcal{R}|$ , and  $P = |\mathcal{T}|^2 + |\mathcal{R}|^2$ . (b) The mean and variance of phase spectrum for the entire dataset.

### 3.3. Peak locations in the spectrum

In some applications such as filtering [42], the locations of peaks in a spectrum are important. One way to extract the locations of peaks is to convert it to the sum of the Pearson Type VII function [48], which will reduce the dimension of the output EM response from 1001 to  $4N + 2$ , where  $N$  is the number of peaks. However, it may not retain the locality information and unable to recover exactly the spectrum after the transformation. Note that the magnitude spectra for PLG, PTN, and PLR classes are usually smooth, so these three classes are not suitable for experimentation of this approach. The magnitude spectra for RDN class of metasurfaces contains more peaks, which is used for this testing. From the RDN class, it is found that there is at most six peaks ( $N = 6$ ) between 2 to 12 GHz, and thus the output of the model can be greatly compressed to only 26 (compared to 1001). The general fitting function used is

$$C(x) = o + k * x + \sum_i^{Peaks} a_i \left[ 1 + \frac{(x - d_i)^2}{b_i^2} \right]^{-m_i}$$

where  $d_i \in [2, 12]$ ,  $a_i \in [0, 1]$ ,  $b_i \in [0, 5]$ ,  $m_i \in [1, 6]$ .

Figure 4a illustrates an example of the decomposition of an arbitrary magnitude spectrum,  $|\mathcal{R}|$  with three peaks. The parameters,  $a_i$  and  $b_i$ , measure respectively the heights and widths of a peak. Fig. 4b shows the distributions of height ( $a_i$ ) and width ( $b_i$ ) of all the samples in the RDN class of our dataset. This proposed mathematical transformation has the advantage that the fitting parameters,  $a_i$ ,  $b_i$ , and  $m_i$  are more robust against noise, which do not require high precision. In contrast, the location parameter ( $d_i$ ) is critical. In order to obtain the accurate peak location, it is desirable to formulate a classification problem as compared to a regression problem. In this case, a metasurface can be associated with multiple labels. Each label,  $i$ , belongs to integer

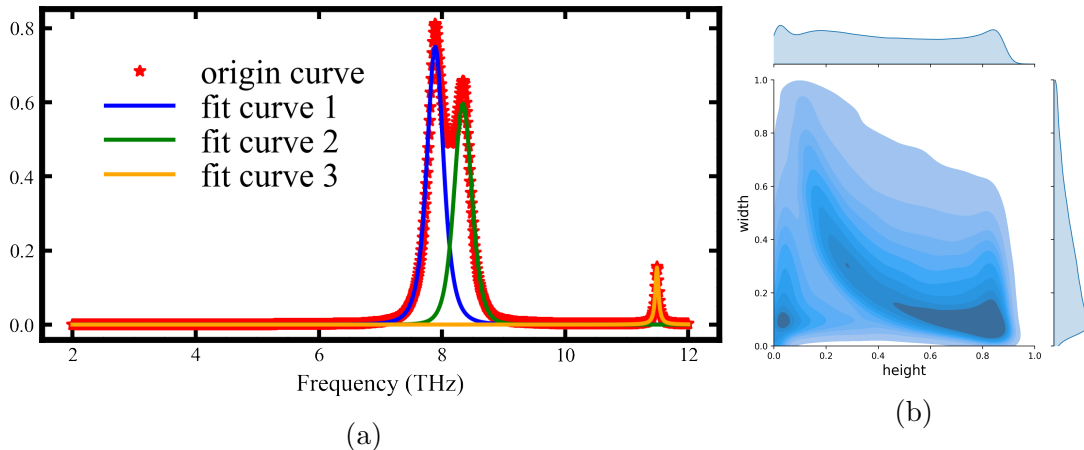


Figure 4: (a) A demonstration of peak decomposition performed on a magnitude spectrum using the Pearson Type VII function and the resulting 3 peaks. (b) The statistical distribution of heights ( $a_i$ ) and widths ( $b_i$ ) of the peaks extracted from the magnitude spectra,  $|\mathcal{R}|$ , for all metasurfaces in the RDN class. With the hotspot concentrating at the bottom right region, it is observed that the peaks are mostly distinctive sharp peaks. The peak decomposition is an effective method for extracting peak characteristics of the spectra.

values between 1 to 1001. To identify the peaks,  $i$  will be used to index into the discrete frequencies between 2 to 12 GHz. In general, multi-label classification problem can be challenging. For simplicity, we consider a binary classification problem, which we term as maximum peak binary classification (MPBC) task. In this learning task, we determine whether the location of the maximum peak is located at a position larger than a given threshold of frequency. If this occurs, the associated input metasurface is assigned a positive label. Otherwise, the input metasurface is assigned a negative label. To avoid bias in MPBC, it is desirable to have balanced classes, i.e. both positive and negative classes possess approximately equal number of training data. Successfully dealing with this task will help to extend the problem to a multi-label classification setting. Alternatively, by design, multi-label classification can be realized by cascading multiple binary classifiers. In the following section, we will demonstrate the application of NAS using this MPBC problem.

#### 4. NAS for high performance neural architecture

In this section, we will consider the MPBC problem on RDN class mentioned above. For benchmarking purpose, we adopt some off-the-shelf models including traditional ML models and popular DL models in CV community, and NAS will be implemented to compare with these models.

#### 4.1. Benchmark with existing ML models

The benchmarking task here is to predict whether the maximum peak in a spectrum is located at a frequency larger than a threshold frequency. If the maximum peak is at frequency larger than the threshold, the binary image is assigned a positive label, otherwise, a negative label. The threshold frequency is selected to be 8.3 GHz, which is the median frequency as shown in the histogram in Fig. 5. Focusing on the RDN class of SUTD-PRCM dataset and extracting the peak information for MPBC, a label either positive or negative can then be assigned to a metasurface pattern. RDN class has 110,000 samples, where 108,000 are used as training samples, and 2000 are as test samples. In the training dataset, there are 55,364 positive labels and 52,636 negative labels. In the test dataset, there are 1508 positive labels and 1492 negative labels. The classification accuracy is a popular metric to assess the performance of the classification models. A simple baseline classifier which always predicts the same label can produce a baseline accuracy of  $1508/3000 = 50.27\%$  due to roughly equal positive and negative classes in the training dataset.

In comparison, we have applied traditional machine learning models such as random forest classifier (RFC) and linear/log support vector machine (SVM) classifier. However, the results are only marginally better than the baseline accuracy, i.e. RFC and SVM is about 53% and 55%, respectively. The location of maximum peak cannot be well identified with these ML models. Considering our RDN class of datasets resembles images, we apply some off-the-shelf neural network architectures, such as deep multi layer perception (MLP), Resnet18 (RS18), Resnet34 (RS34), and SqueezeNet (SQN1) to tackle this problem. These architectures are well known to perform excellent with CV related tasks, and they have been adapted to accommodate the image size in the dataset and trained from scratch. To our surprise, all these neural network models do not score above 60% accuracy as shown in Fig.6. Notice that another model labelled DARTS is included in the same figure, which performs significantly better. This model is based on neural architecture search (NAS) that we will elaborate in the next section. Note

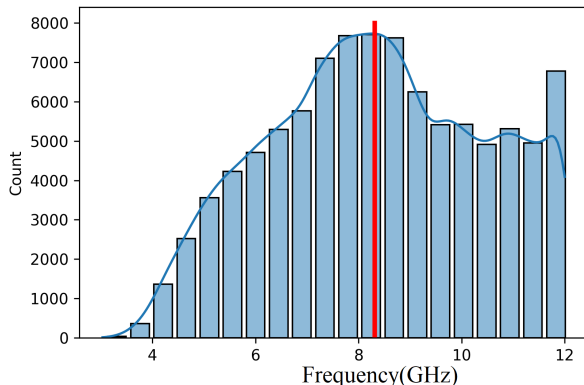


Figure 5: The histogram of location of maximum peak in the magnitude spectra,  $|\mathcal{R}|$ , of RDN class of metasurface.

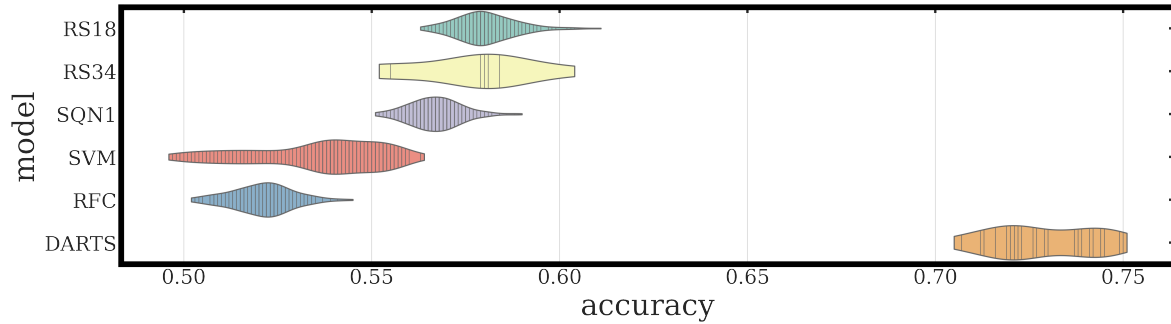


Figure 6: Every scattering point is representing one trial with different hyper parameters. Different colors represent different machine learning models. Each model is trained to converge. The five models (on the left) are the traditional machine learning models listed from top to bottom: RS18 (Resnet18s), RS34 (Resnet34S), SQN1 (SqueezeNet1S), SVM (Support Vector Machine), RFC (Random Forest Classification machine). The last one on the right is the best NAS based model (DARTS), which holds the state-of-the-art performance in MPBC task.

in our prior work [44], a modified version of Resnet18 was reported to achieve excellent performance in a related regression problem formulated to predict EM response of the RDN class in SUTD-PRCM dataset.

The low accuracy (less than 60%) certainly is not appealing and definitely signifies more research to be done. For comparison, we applied the same set of ML/DL models to a scaled binarized MNIST dataset, which is a well studied handwritten digit dataset. Traditional ML models can achieve over 90% accuracy: SVM (91%) and RFC (96.9%). DL models can achieve over 95% accuracy: SqueezeNet1S (95.5%), Resnet18S (96%), DARTS (97%), and Resnet34S (98.5%). As of writing, the best DL model on the standard MNIST dataset is Efficient-CapsNet [49], which can attain a classification accuracy of 99.9%. Such a good performance is credited to decades of effort from ML community in testing on the same common dataset, which reinforces the importance of having a common dataset for metasurfaces if an optimal DL model is aimed to be developed for the design of complex metasurfaces. Thus, this motivates us to share our dataset (SUTD-PRCM) in this paper.

While the classification problem using RDN class here might appear to be similar as compared to MNIST dataset, and one may wonder if an accuracy of over 90% is possible using the known DL models. However, we emphasize here the significant differences between random metasurfaces (RDN) and handwritten digits (MNIST). Each image of MNIST is a centralized and continuous image. Furthermore, each digit (0-9) can smoothly deform to each other. This restricts the possible patterns to a small subset of the domain of a  $16 \times 16$  binary image. Contrary to the MPBC problem, the input pattern can be any random binary  $16 \times 16$  image. Apparently, the complexity of MPBC problem studied here in using our dataset is higher than that of the MNIST digit recognition. With the initial findings from [44], we speculate that the architecture of

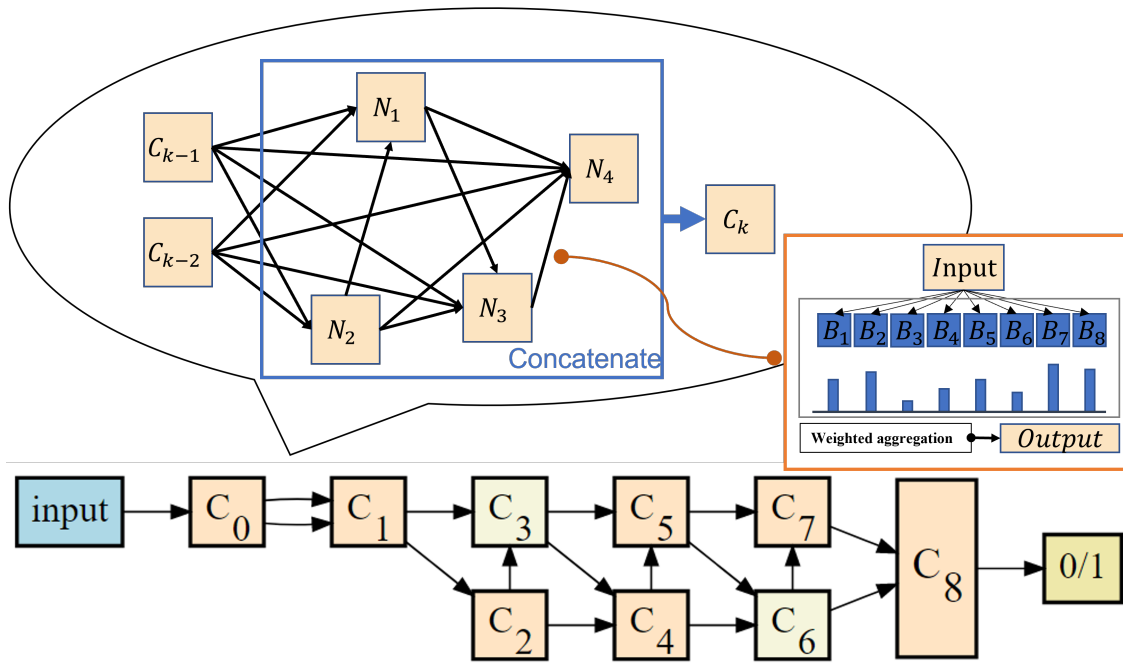
the existing neural network used for SUTD-PRCM dataset might not be optimal yet. In the following section, we demonstrate further improvements in this direction.

#### 4.2. Neural architecture search

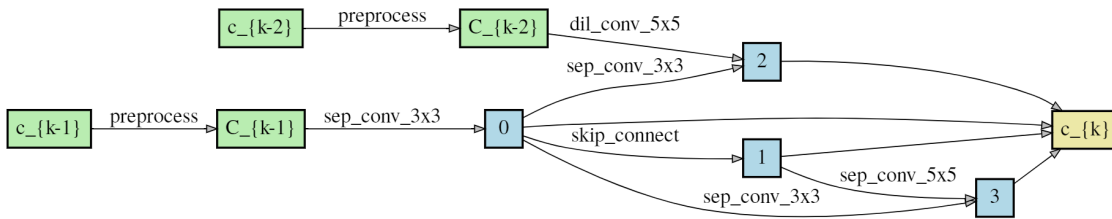
Neural architecture search (NAS) is certainly not a new concept but it has just become an affordable tool in everyone’s ML toolbox. In fact, NAS is a follow-up idea to automate the laborious effort to design optimal neural architecture for any given problem in DL. Early attempts has resorted to huge amount of computational resources that only big enterprises or research groups can afford. It is not until recently that one can perform NAS on a common workstation [50–53].

The objective of NAS is to discover the best architecture for a neural network tailored for a specific requirement based on a given dataset. It essentially takes the process of a human manual process in modifying neural network for better performance. Thus NAS is an automated discovery of more optimal network architectures for a given dataset. It represents a set of tools and methods that will test and evaluate a large number of architectures across a search space using a search strategy in order to select the one that is most suitable for a given problem by maximizing a fitness function. The most well-known NAS method is the Google’s NASNet [50], but this method requires thousands of TPU/GPU resources that are not affordable for common research groups. In the rapid advancement of NAS, researchers have put forward many experimental NAS methods like Reinforcement Learning (RL) Methods [51], Gradient-based (GB) Methods [52], Evolutionary Algorithms (EA) [54] and Bayesian Optimization (BO) [53]. In this section, we adopt the Differentiable Architecture Search (DARTS) with Geometry-Awared gradient algorithm [52, 55, 56] as it requires significantly less computational resources as compared to other NAS methods. Unlike the RL or EA approaches, DARTS introduces a continuous relaxation scheme that enables differentiable learning objective. This differentiability is the key to the computational feasibility following a gradient based approach. In our experiment, we inherit the spirit of [52] and update the architecture following a geometry strategy [55], which helps us to converge quickly and escape from the local minima. The full search space is shown in Fig. 7a. It is noted that we modify some configurations to adapt to the MPBC problem. The candidate architecture finally converges into a relatively simple structure shown in Fig. 7b and Fig. 7c.

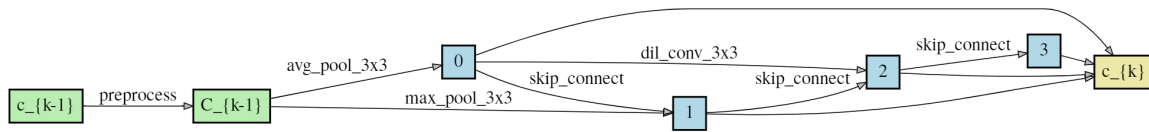
Our finding shows the NAS based DARTS model is able to achieve an accuracy over 75% as shown in Fig.6, which surpasses all the ML models in our experiment. This optimal network architecture suggested by NAS-DARTS requires 233,682 parameters, which is only about 1/5 and 1/10 of the requirements from Resnet18S and Resnet34S, respectively [see Table 2]. Intuitively, more parameters that accompanying by a bigger model provide better capability to capture the inherent relationship between inputs and outputs. Surprisingly, the NAS-DARTS approach suggests an alternative shallow and smaller architecture to achieve better performance than the other models. Table 2 shows



(a) Main structure containing normal (orange) and reduce (yellow) branch.



(b) Normal branch.



(c) Reduce branch.

Figure 7: (a) The main structure of the network architecture search (NAS) module. The orange and yellow square represent the two architectural types respectively. There are nine cells from  $C_0$  to  $C_8$ . Each cell is the interaction of the last two cells. The interaction contains 4 intermediate units ( $N_1$  to  $N_4$ ). Each unit is the sum aggregation of several mapping (black arrow). There are 14 mappings in one interaction. Each mapping is a weighted aggregation of candidate operations. In this paper, we use eight symmetry operations  $S_i$ . A final linear layer is applied to convert  $C_8$  to the binary output of positive 1 or negative 0. (b) and (c) are the final truncated architecture produced by NAS. Only the first and the second important path are kept for each node.

Table 2: The comparison between different neural architectures and NAS based neural architecture. The parameters are referring to the total free parameters in all operations. For example, convolution with kernel size  $(C_2, C_1, w, h)$  is one operation with  $w \times h \times C_1 \times C_2$  parameters.

Model	No. Operations	No. Parameters
<b>SqueezeNet1S</b>	51	742306
<b>MLP</b>	30	5659074
<b>Resnet18S</b>	62	11174338
<b>Resnet34S</b>	110	21282498
<b>DARTS</b>	194	232034

a comparison of the number of parameters and operations of different models used in the SUTD-PRCM (RDN Class) dataset.

The trainable parameters of the DARTS model are much less than the traditional DL model, but it has double or triple the operation numbers, which highlights the importance of a suitable neural network architecture. Designing a suitable meta-operation may be more effective than building an arbitrary large and deep neural network architecture. The detailed structure of our NAS-based DL model (Fig.7) has shown that convolution stacking is not the dominant element of the architecture anymore, which implies that low-level features are preferred over deep hierarchical high-level features (that are common for traditional CNN), thus explains why the CNN based models like Resnet and SqueezeNet are not performing well in this SUTD-PRCM dataset studied in this paper.

## 5. Conclusion

We have presented our home-made SUTD-PRCM dataset based on numerical EM simulations of metasurfaces that contains EM spectral responses associated with complex metasurface patterns, which are divided into four classes having different properties. This dataset has been tested in a prior work [44] and we postulate that existing CNN based DL models is likely not the optimal architecture yet. Thus we are sharing this dataset with the community for further improvement. This SUTD-PRCM may also be used as a common dataset of random metasurfaces for more quantitative performance comparison between different models and training strategies.

In the second part of the paper, we discuss a binary classification problem formulated based on this dataset. By using the Differentiable Architecture Search (DARTS) based neural architecture search (NAS) method, we show the improvement over the traditional ML methods and off-the-shelf DL models (popular in the computer vision community) such as Resnet and SqueezeNet. Based on NAS-DARTS results, this SUTD-PRCM dataset prefer shallow and wide neural networks for better prediction. With modern approach of inverse design often features a fast surrogate model in terms of DNN,

this finding has profound impact on the design applications of complex metasurfaces as well. In future work, one can probably improve by fine-tuning the NAS method, which is beyond the scope of this paper. In particular, making tradeoff for search space of neural architecture can be tedious and frustrating. Through performing exploratory analysis with this physics-based SUTD-PRCM dataset, we also hope to alleviate some of the difficulties and this will be investigated in our future works, including in using complex number based DL models.

### **Data availability statement**

The data that support the findings of this study are openly available at the following URL/DOI: [https://github.com/veya2ztn/SUTD\\_PRCM\\_dataset](https://github.com/veya2ztn/SUTD_PRCM_dataset)

### **Acknowledgments**

This work was supported by USA Office of Naval Research Global (N62909-19-1-2047) and SUTD-ZJU Visiting Professor (VP 201303). T.Z acknowledges the support of Singapore Ministry of Education PhD Research Scholarship. Y.S.A. acknowledges the support of SUTD Start-Up Research Grant (SRT3CI21163).

**References**

- [1] Oscar Quevedo-Teruel, Hongsheng Chen, Ana Díaz-Rubio, Gurkan Gok, Anthony Grbic, Gabriele Minatti, Enrica Martini, Stefano Maci, George V Eleftheriades, Michael Chen, et al. Roadmap on metasurfaces. *Journal of Optics*, 21(7):073002, 2019.
- [2] Rujia Li, Zuoqia Wang, and Hongsheng Chen. *Metamaterials and Negative Refraction*. Cambridge University Press, 2020.
- [3] Zhipeng Li, Xi Tian, Cheng-Wei Qiu, and John S Ho. Metasurfaces for bioelectronics and healthcare. *Nature Electronics*, pages 1–10, 2021.
- [4] Tie Jun Cui, Shuo Liu, and Lei Zhang. Information metamaterials and metasurfaces. *Journal of Materials Chemistry C*, 5(15):3644–3668, 2017.
- [5] Ying Li, Wei Li, Tiancheng Han, Xu Zheng, Jiabin Li, Baowen Li, Shanhui Fan, and Cheng-Wei Qiu. Transforming heat transfer with thermal metamaterials and devices. *Nature Reviews Materials*, 6(6):488–507, 2021.
- [6] Yihao Yang, Liqiao Jing, Bin Zheng, Ran Hao, Wenyan Yin, Erping Li, Costas M Soukoulis, and Hongsheng Chen. Full-polarization 3d metasurface cloak with preserved amplitude and phase. *Advanced Materials*, 28(32):6866–6871, 2016.
- [7] Chao Qian and Hongsheng Chen. A perspective on the next generation of invisibility cloaks—intelligent cloaks. *Applied Physics Letters*, 118(18):180501, 2021.
- [8] Che Liu, Qian Ma, Lianlin Li, and Tie Jun Cui. Work in progress: Intelligent metasurface holograms. In *Proceedings of the 1st ACM International Workshop on Nanoscale Computing, Communication, and Applications*, pages 45–48, 2020.
- [9] Chuanbao Liu, Yang Bai, Qian Zhao, Yihao Yang, Hongsheng Chen, Ji Zhou, and Lijie Qiao. Fully controllable pancharatnam-berry metasurface array with high conversion efficiency and broad bandwidth. *Scientific reports*, 6(1):1–7, 2016.
- [10] Oleg Mitrofanov, Thomas Siday, Robert J Thompson, Ting Shan Luk, Igal Brener, and John L Reno. Efficient photoconductive terahertz detector with all-dielectric optical metasurface. *APL Photonics*, 3(5):051703, 2018.
- [11] Oleg Mitrofanov, Lucy L Hale, Polina P Vabishchevich, Ting Shan Luk, Sadvikas J Addamane, John L Reno, and Igal Brener. Perfectly absorbing dielectric metasurfaces for photodetection. *APL Photonics*, 5(10):101304, 2020.
- [12] Haoyang Zhang, Qiao Cheng, Hongchen Chu, Orestis Christogeorgos, Wen Wu, and Yang Hao. Hyperuniform disordered distribution metasurface for scattering reduction. *Applied Physics Letters*, 118(10):101601, 2021.
- [13] Muhammad Ismail Khan, Qaisar Fraz, and Farooq A Tahir. Ultra-wideband cross polarization conversion metasurface insensitive to incidence angle. *Journal of Applied Physics*, 121(4):045103, 2017.

- [14] Mohammadreza Khorasaninejad, Wei Ting Chen, Robert C Devlin, Jaewon Oh, Alexander Y Zhu, and Federico Capasso. Metalenses at visible wavelengths: Diffraction-limited focusing and subwavelength resolution imaging. *Science*, 352(6290):1190–1194, 2016.
- [15] Mohammadreza Khorasaninejad and Federico Capasso. Metalenses: Versatile multifunctional photonic components. *Science*, 358(6367), 2017.
- [16] Xiaolong You, Rajour T Ako, Wendy SL Lee, Madhu Bhaskaran, Sharath Sriram, Christophe Fumeaux, and Withawat Withayachumnankul. Broadband terahertz transmissive quarter-wave metasurface. *APL Photonics*, 5(9):096108, 2020.
- [17] Fei Cheng, Jie Gao, Ting S Luk, and Xiaodong Yang. Structural color printing based on plasmonic metasurfaces of perfect light absorption. *Scientific reports*, 5:11045, 2015.
- [18] Julien Proust, Frederic Bedu, Bruno Gallas, Igor Ozerov, and Nicolas Bonod. All-dielectric colored metasurfaces with silicon mie resonators. *ACS nano*, 10(8):7761–7767, 2016.
- [19] Lei Bao, Qian Ma, Rui Yuan Wu, Xiaojian Fu, Junwei Wu, and Tie Jun Cui. Programmable reflection–transmission shared-aperture metasurface for real-time control of electromagnetic waves in full space. *Advanced Science*, page 2100149, 2021.
- [20] Xin Ge Zhang, Qian Yu, Wei Xiang Jiang, Ya Lun Sun, Lin Bai, Qiang Wang, Cheng-Wei Qiu, and Tie Jun Cui. Polarization-controlled dual-programmable metasurfaces. *Advanced science*, 7(11):1903382, 2020.
- [21] Xin Ge Zhang, Wei Xiang Jiang, Hao Lin Jiang, Qiang Wang, Han Wei Tian, Lin Bai, Zhang Jie Luo, Shang Sun, Yu Luo, Cheng-Wei Qiu, et al. An optically driven digital metasurface for programming electromagnetic functions. *Nature Electronics*, 3(3):165–171, 2020.
- [22] Borislav Vasić and Goran Isić. Refractive index sensing with hollow metal–insulator–metal metasurfaces. *Journal of Physics D: Applied Physics*, 54(28):285106, 2021.
- [23] Ronghui Lin, Yanfen Zhai, Chenxin Xiong, and Xiaohang Li. Inverse design of plasmonic metasurfaces by convolutional neural network. *Optics Letters*, 45(6):1362–1365, 2020.
- [24] Ling Yun Niu, Hao Chi Zhang, Pei Hang He, Min Tang, Meini Wang, Guo Dong Bai, Junfa Mao, Tie Jun Cui, et al. Dual-band and dual-polarized programmable metasurface unit with independent channels. *Journal of Physics D: Applied Physics*, 54(14):145109, 2021.
- [25] Mustafa K Taher Al-Nuaimi, Wei Hong, and William G Whittow. Nature-inspired orbital angular momentum beam generator using aperiodic metasurface. *Journal of Physics D: Applied Physics*, 54(27):275106, 2021.

- [26] Omar Khatib, Simiao Ren, Jordan Malof, and Willie J. Padilla. Deep learning the electromagnetic properties of metamaterials—a comprehensive review. *Advanced Functional Materials*, 31(31):2101748, 2021.
- [27] Xin Shi, Tianshuo Qiu, Jiafu Wang, Xueqing Zhao, and Shaobo Qu. Metasurface inverse design using machine learning approaches. *Journal of Physics D: Applied Physics*, 53(27):275105, 2020.
- [28] Abhishek Mall, Abhijeet Patil, Dipesh Tamboli, Amit Sethi, and Anshuman Kumar. Fast design of plasmonic metasurfaces enabled by deep learning. *Journal of Physics D: Applied Physics*, 53(49):49LT01, 2020.
- [29] Ge Ding, Wenjie Xiong, Peipei Wang, Zebin Huang, Yanliang He, Junmin Liu, Ying Li, Dianyuan Fan, and Shuqing Chen. Spatial phase retrieval of vortex beam using convolutional neural network. *Journal of Optics*, 24(2):025701, 2022.
- [30] Xiaoshu Zhou, Qide Xiao, and Han Wang. Metamaterials design method based on deep learning database. In *Journal of Physics: Conference Series*, volume 2185, page 012023. IOP Publishing, 2022.
- [31] Samad Jafar-Zanjani, Sandeep Inampudi, and Hossein Mosallaei. Adaptive genetic algorithm for optical metasurfaces design. *Scientific reports*, 8(1):1–16, 2018.
- [32] Qian Zhang, Xiang Wan, Shuo Liu, Jia Yuan Yin, Lei Zhang, and Tie Jun Cui. Shaping electromagnetic waves using software-automatically-designed metasurfaces. *Scientific Reports*, 7(1), jun 2017.
- [33] Danny Z Zhu, Eric B Whiting, Sawyer D Campbell, D Bruce Burckel, and Douglas H Werner. Optimal high efficiency 3d plasmonic metasurface elements revealed by lazy ants. *ACS Photonics*, 6(11):2741–2748, 2019.
- [34] Itzik Malkiel, Michael Mrejen, Achiya Nagler, Uri Arieli, Lior Wolf, and Haim Suchowski. Plasmonic nanostructure design and characterization via deep learning. *Light: Science & Applications*, 7(1):1–8, 2018.
- [35] John Peurifoy, Yichen Shen, Li Jing, Yi Yang, Fidel Cano-Renteria, Brendan G DeLacy, John D Joannopoulos, Max Tegmark, and Marin Soljačić. Nanophotonic particle simulation and inverse design using artificial neural networks. *Science advances*, 4(6):eaar4206, 2018.
- [36] Sensong An, Clayton Fowler, Bowen Zheng, Mikhail Y Shalaginov, Hong Tang, Hang Li, Li Zhou, Jun Ding, Anuradha Murthy Agarwal, Clara Rivero-Baleine, et al. A deep learning approach for objective-driven all-dielectric metasurface design. *ACS Photonics*, 6(12):3196–3207, 2019.
- [37] Dianjing Liu, Yixuan Tan, Erfan Khoram, and Zongfu Yu. Training deep neural networks for the inverse design of nanophotonic structures. *ACS Photonics*, 5(4):1365–1369, 2018.
- [38] Takashi Asano and Susumu Noda. Optimization of photonic crystal nanocavities based on deep learning. *Optics express*, 26(25):32704–32717, 2018.

- [39] Jiaqi Jiang, David Sell, Stephan Hoyer, Jason Hickey, Jianji Yang, and Jonathan A Fan. Free-form diffractive metagrating design based on generative adversarial networks. *ACS nano*, 13(8):8872–8878, 2019.
- [40] Jiaqi Jiang and Jonathan A Fan. Global optimization of dielectric metasurfaces using a physics-driven neural network. *Nano letters*, 19(8):5366–5372, 2019.
- [41] Ian Goodfellow, Jean Pouget-Abadie, Mehdi Mirza, Bing Xu, David Warde-Farley, Sherjil Ozair, Aaron Courville, and Yoshua Bengio. Generative adversarial nets. In *Advances in neural information processing systems*, pages 2672–2680, 2014.
- [42] Xiao Han, Ziyang Fan, Zeyang Liu, Chao Li, and L Jay Guo. Inverse design of metasurface optical filters using deep neural network with high degrees of freedom. *InfoMat*.
- [43] Iman Sajedian, Jeonghyun Kim, and Junsuk Rho. Finding the optical properties of plasmonic structures by image processing using a combination of convolutional neural networks and recurrent neural networks. *Microsystems & nanoengineering*, 5(1):1–8, 2019.
- [44] Tianning Zhang, Chun Yun Kee, Yee Sin Ang, and L. K. Ang. Deep learning-based design of broadband ghz complex and random metasurfaces. *APL Photonics*, 6(10):106101, 2021.
- [45] Zhaocheng Liu, Dayu Zhu, Sean P Rodrigues, Kyu-Tae Lee, and Wenshan Cai. Generative model for the inverse design of metasurfaces. *Nano letters*, 18(10):6570–6576, 2018.
- [46] Joshua Basse, Lijun Qian, and Xianfang Li. A survey of complex-valued neural networks, 2021.
- [47] Joan Bruna and Stéphane Mallat. Invariant scattering convolution networks. *IEEE transactions on pattern analysis and machine intelligence*, 35(8):1872–1886, 2013.
- [48] SK Gupta. Peak decomposition using pearson type vii function. *Journal of applied crystallography*, 31(3):474–476, 1998.
- [49] Vittorio Mazzia, Francesco Salvetti, and Marcello Chiaberge. Efficient-capsnet: Capsule network with self-attention routing. *Scientific Reports*, 11(1):1–13, 2021.
- [50] Xu Qin and Zhilin Wang. Nasnet: A neuron attention stage-by-stage net for single image deraining. *arXiv preprint arXiv:1912.03151*, 2019.
- [51] Barret Zoph and Quoc V Le. Neural architecture search with reinforcement learning. *arXiv preprint arXiv:1611.01578*, 2016.
- [52] Hanxiao Liu, Karen Simonyan, and Yiming Yang. Darts: Differentiable architecture search. *arXiv preprint arXiv:1806.09055*, 2018.
- [53] Kirthevasan Kandasamy, Willie Neiswanger, Jeff Schneider, Barnabas Poczos, and Eric Xing. Neural architecture search with bayesian optimisation and optimal transport. *arXiv preprint arXiv:1802.07191*, 2018.
- [54] Esteban Real, Sherry Moore, Andrew Selle, Saurabh Saxena, Yutaka Leon Suematsu, Jie Tan, Quoc V Le, and Alexey Kurakin. Large-scale evolution of

- image classifiers. In *International Conference on Machine Learning*, pages 2902–2911. PMLR, 2017.
- [55] Liam Li, Mikhail Khodak, Maria-Florina Balcan, and Ameet Talwalkar. Geometry-aware gradient algorithms for neural architecture search. *arXiv preprint arXiv:2004.07802*, 2020.
- [56] Yuhui Xu, Lingxi Xie, Xiaopeng Zhang, Xin Chen, Guo-Jun Qi, Qi Tian, and Hongkai Xiong. Pc-darts: Partial channel connections for memory-efficient architecture search. *arXiv preprint arXiv:1907.05737*, 2019.